Synthesis of eco-compatible bimetallic silver/iron nanoparticles for water remediation and reactivity assessment on bromophenol blue

Synthesis of eco-compatible bimetallic silver/iron nanoparticles for water remediation and reactivity assessment on bromophenol blue

Andrea Gallo[a], Carlo Bianco [a], Tiziana Tosco[a], Alberto Tiraferri[a] and Rajandrea Sethi[a,*]

[a] Department of environmental, land and infrastructure engineering, Politecnico di Torino, C.so Duca degli Abruzzi 24, 10129 Turin – ITALY

andrea.gallo@polito.it ; carlo.bianco@polito.it ; tiziana.tosco@polito.it ; alberto.tiraferri@polito.it ; rajandrea.sethi@polito.it

* Corresponding author, TEL +39 011 0907601

Abstract

In the last decade, zero-valent iron nanoparticles (nZVI) have been applied for groundwater remediation and they proved to be effective towards a wide range of organic and inorganic contaminants. One of the critical aspects related to the synthesis of this material concerns the use of borohydride, which increases the cost of the final product and generates toxic borates. This study presents a new benign synthesis method to produce bimetallic nanoscale zero-valent silver/iron (nZVSI). The properties and the reactivity towards a model compound of the resulting material are thus discussed. The novel synthesis protocol employs hydrosulfite as reducing agent and it is of easy implementation and scalability. The bimetallic nanoparticles have narrow size distribution and show appropriate colloidal stability. They consist of a core of zerovalent iron and a thin shell of iron oxide, while silver is homogeneously distributed within the material. The nanoparticles degraded bromophenol blue with suitable kinetics and using a low amount of material. Additionally, the bimetallic nanomaterial significantly outperformed nanometric zero-valent silver (nZVS) and nZVI obtained with the same protocol. The proposed synthesis would allow to significantly reduce the environmental and health impact of the stage prior to product injection into the subsoil. Also, the simplicity and the safety of the proposed synthesis procedure would allow the production of the bimetallic reactant directly on-site, thus streamlining the remediation process and maximizing its efficiency.

Keywords

Nanotechnology, groundwater remediation, zero-valent iron, nanoparticle synthesis, bimetallic nanoparticles

1. INTRODUCTION

Over the last years, remediation technologies based on reactive or sorptive nanomaterials have proven highly efficient against a wide spectrum of pollutants (Bates et al., 2016; Maretto et al., 2015; Minella et al., 2016; Sadik et al., 2014; Yin et al., 2018). In the field of groundwater remediation, zero-valent iron (ZVI) has been applied as a strong reducing agent towards many organic contaminants (Tosco et al., 2014; Zhang, 2003) and heavy metals (Cox and Durant, 2005; Hashim et al., 2011; Sadik et al., 2014). Initially applied as millimetric particles in permeable reactive barriers (PRBs) (Di Molfetta and Sethi, 2006), ZVI is currently used in nanometric form, namely nZVI. Such reduction in size results in *i)* better removal performance due to the corresponding increase in surface area, and ii) easier deployment by means of injection of stable suspensions (Saleh et al., 2007; Tosco et al., 2014). Such technology has now been thoroughly tested and is already applied for large scale contaminated sites. One of the most significant aspects (Tosco et al., 2014) limiting a faster and wider diffusion of this technology, especially in Europe (Mueller et al., 2012), is the cost associated to the synthesis of nZVI (Crane and Scott, 2012; Kozma et al., 2016).

The initial top-down methods to synthesize nanoscale zero-valent iron required the production of bulk ZVI and its milling to proper size (1-100 nm according to ISO definition of “nano”) (Cary and Hybinette, 1947; Stefaniuk et al., 2016). This approach was associated with high costs and required adequate facilities. At present time, most procedures employ chemical reduction of ferrous/ferric salt solutions, directly leading to the formation of nanosized particles (Harutyunyan et al., 2005; Zhao et al., 2016). The choice of the reducing agent is dictated by the reduction potential of the salts chosen as precursors of Fe(0). The approach currently applied for the industrial production of nZVI uses a strong but highly toxic reducing agent, namely, sodium borohydride (Kozma et al., 2016; Stefaniuk et al., 2016; Tosco et al., 2014). This reaction is carried out in an alkaline medium to maximize the standard reducing potential E_0 (Schaeffer et al., 1961) and to minimize borohydride decomposition (Schlesinger et al., 1953), hence the resulting nZVI presents an excellent reactivity (Hwang et al., 2011; Ma et al., 2016). However, sodium borohydride is an expensive chemical, and its use requires cumbersome safety measures dictated by the related production of borates and hydrogen (Fu et al., 2014; Stefaniuk et al., 2016). The presence of hydrogen requires an efficient air recirculation to avoid reaching the critical explosive mixing ratio with air (4-74%). Of greater concern is the production of borates, which are classified as toxic for organism reproduction (or reprotoxic) (Duydu et al., 2016; Heindel et al., 1994). The production of toxic compounds strongly interferes with the beneficial aspects of nZVI application in nanoremediation, imposing the need of a post-treatment to remove such contaminants before the product is delivered into the environment. In addition, boron and boron compounds removal

from water cannot be achieved by biological treatment or by coagulation with metal salts (Remy et al., 2005). Other methods are available, such as ion exchange resins, precipitation of insoluble salts, or reverse osmosis (Di Vincenzo et al., 2017), but these separation methods require specific conditions (e.g., pH, boron concentration) to be cost effective (Xu and Jiang, 2008). Such processes lead therefore to higher costs and might affect the performance of the material, as they often promote nZVI oxidation (Hwang et al., 2011).

To find less toxic alternatives to borohydride, some authors (Fazlzadeh et al., 2017; Kumar et al., 2015; Mystrioti et al., 2016) identified plant extracts containing high quantities of natural antioxidants (e.g., polyphenols, aldehydes and ketones, reducing sugars) as alternative eco-compatible reducing agents. Such compounds are separated from the raw material by means of thermal extraction in water at abt. 80 °C. However, since their E_0 is much lower than borohydride (Novak Jovanović and Miličević, 2017; Schaeffer et al., 1961), high quantities of raw plant material, up to 300 g/L, are needed to process relatively small quantities of iron salts (Kozma et al., 2016; Sunardi et al., 2017). Another approach in finding alternatives to borohydride is using other inorganic reducing agents with lower, or negligible, environmental impact. In this perspective, sodium hydrosulfite (also known as sodium dithionite or hypodisulfite) is already applied to promote in-situ chemical reduction (Hashim et al., 2011; Li et al., 2018). Following the same principle, it can also be applied to obtain zero-valent metals from their salts without leading to harmful byproducts, but only water and sodium sulfate (Ma et al., 2016).

The purpose of this study is to devise a cheap and eco-compatible protocol, of easy implementation even on-site, to produce a zero-valent iron based reactive material. Such protocol is simple and scalable, as it uses hydrosulfite in open vessel reactors and unmodified medium (i.e., non-degassed water and non-inert atmosphere). The goal is to obtain a material with suitable pollutant removal performance in terms of kinetics and efficiency, which is expected to be achieved by synthetizing a ZVI-based material doped with a noble metal. While the use of palladium or platinum is known to significantly improve the efficiency of nZVI, the suggested approach aims to reduce synthesis costs by employing silver, a cheaper noble metal that may also provide antibacterial properties to the final product. Also, to reduce the technical complexity of the process, the doping is implemented during and not after the synthesis of nZVI, using ZVI itself as a reductant. Based on the standard potentials, operating a concomitant reduction is expected to generate a redox potential of the reaction medium more favourable for nZVI stability. Although this method is only partly green, it leads to the significant reduction of the environmental impacts of the final product, as it prevents the formation of toxic byproducts at the last stage of the production process. To assess the validity of our assumption on the

synthesis efficacy, the performance of the bimetallic material to degrade bromophenol blue is discussed and compared with the respective mono-metallic particles (i.e., zero-valent iron, ZVI and zero-valent silver, ZVS) obtained with the same protocol.

2. MATERIALS AND METHODS

For the nZVSI synthesis, iron sulfate heptahydrate (CAS 7782-63-0, purity ≥99%), silver nitrate (CAS 7761-88-8, purity ≥99.99%), sodium hydroxide pellets (CAS 1310-73-2, analytical grade), sodium hydrosulfite (CAS 7775-14-6, purity ≥82%) were used. The reactivity tests were carried out on bromophenol blue (BPB, CAS 115-39-9, ACS grade). All reagents were purchased from Sigma-Aldrich, and all the solutions were prepared just prior to the synthesis and reactivity tests in ultrapure deionized water (DIW) using clean and dry glassware.

2.1. Synthesis procedure

The syntheses of the materials were conducted in open vessel reactors under mechanical stirring at 600 rpm, constant for the whole test duration. The addition of reagents was operated manually using syringes, timing the addition rate with a timer. For the synthesis of nanoscale zero-valent silver/iron (nZVSI), $AgNO_3$ (10 mM), $FeSO_4 \cdot 7H_2O$ (37 mM) stock solutions were prepared in ultrapure DIW, while a $Na_2S_2O_4$ (58 mM) stock solution was prepared in a NaOH solution at pH 13. As for borohydride, alkaline pH prevents hydrosulfite decomposition (Münchow and Steudel, 1994) and improves the standard reduction potential.(Chao, 1986) The synthesis was carried out with a ratio Fe:Ag=5.5, while hydrosulfite was added with a 50% excess with respect to the stoichiometric quantity to completely reduce all the metal salts. The reagents were added sequentially as follows: *i)* addition of a first aliquot of hydrosulfite, *ii)* addition of silver nitrate, *iii)* addition of iron sulfate, *iv)* addition of a second aliquot of hydrosulfite. Events were spaced by two minutes. After the last addition of hydrosulfite, the solution was stirred for five minutes to complete the reduction process.

To obtain zero-valent iron nanoparticles (nZVI), step *ii* was omitted from the protocol for nZVSI, while the amount of hydrosulfite was left unchanged. At the end of the synthesis, an aliquot of DIW was added to obtain the same final volume as for the nZVSI suspension. Similarly, to obtain zero-valent silver (ZVS), step *iii* was omitted from the protocol, and the amount of hydrosulfite was left unchanged. At the end of the synthesis, an aliquot of DIW was added to obtain the same final volume as for the nZVSI suspension.

2.2. Material characterization

Dimensional analysis of all particles was performed with a Malvern Zetasizer Nano-Z DLS on a sonicated suspension. Before the analysis, the product was rinsed five times with DIW, re-suspending the particles in each step to remove most reagent residues. Further characterization was carried out using transmission electron microscopy (JEM 3010 – JEOL) on a sample of washed nZVSI dried on a copper mesh-grid. The micrographs were analysed with ImageJ software (Schneider et al., 2012).

The chemical characterization of nZVSI was conducted by means of X-ray photoelectron spectroscopy (XPS, PHI Scanning X-ray Microprobe Al Kα radiation). The sample was deposited wet in the analysis chamber and dried in vacuum to minimize oxidation, calibration was obtained on adventitious carbon at 284.6 eV. The oxide layer thickness was calculated using the model proposed by Martin et al. (2008). To explore the bulk composition of the material, a one-minute cleaning etch with Ar^+ was performed, thus repeating the analysis. The cleaning step was repeated twice to obtain a more detailed concentration depth-profile.

2.3. Evaluation of reactivity

Before testing their reactivity, all the materials were washed thoroughly to remove reductant residues, which may otherwise contribute to the substrate degradation, hence leading to overestimation of the decolorization efficiency. To assess the success of this step, a control test was carried out adding 0.5 mL supernatant to a BPB solution and monitoring its change in absorbance over time. The reactivity assessment was carried out in batch reactors, using a 25 mg/L (0.037 mM) BPB solution. Each explored reaction time was obtained from a separate batch experiment to prevent the possible alteration of the conditions during the degradation process due to sampling. Multiple tests were carried out increasing the amount of reactive particles in the BPB solution (0.2; 0.4; 0.8; 2; 4 g/L) to determine the effect of nanoparticle concentration on decolorization. With this protocol, both the kinetics constant and the removal capacity per mass unit of material were determined. The same protocol was also applied to nZVI and ZVS using 0.8 g/L as nanoparticle concentration, to compare their performance with that of nZVSI. All the samples were analysed with an Analytik-Jena SpecordS600 spectrophotometer in Suprasil quartz cuvettes (Hellma Analytics).

3. RESULTS AND DISCUSSION

3.1. Material synthesis

During the nZVSI synthesis the formation of silver nanoparticles in step *ii* was marked by a change in the solution from colourless to yellow, progressing then from dark brown to grey at the end of the reaction. As soon as the iron solution was added, the colour turned olive green and then rapidly to dark grey due to the formation of zero-valent iron. The reaction yield (with respect to the total metal reduction) resulted to be abt. 85-90%. Similar yields were observed for the synthesis of nZVI and ZVS, the latter showing rapid agglomeration that led to a micrometric material rather than nanoparticles. Variations to the protocol (stirring and reactant addition velocity) did not significantly improve the synthesis in terms of particle size.

3.2. Dimensional and morphological properties

The DLS analysis of freshly synthetized nZVSI allowed the determination of the hydrodynamic diameter. The size distribution was bimodal in both intensity (Figure 1a) and number (Figure 1b) distribution, with two peaks centred at 33±3 nm and 122±3 nm. The relative abundance of the peak in the nanometric range (33 nm), which was obtained with peak integration, was 3.2% in intensity and 98% in number distribution.

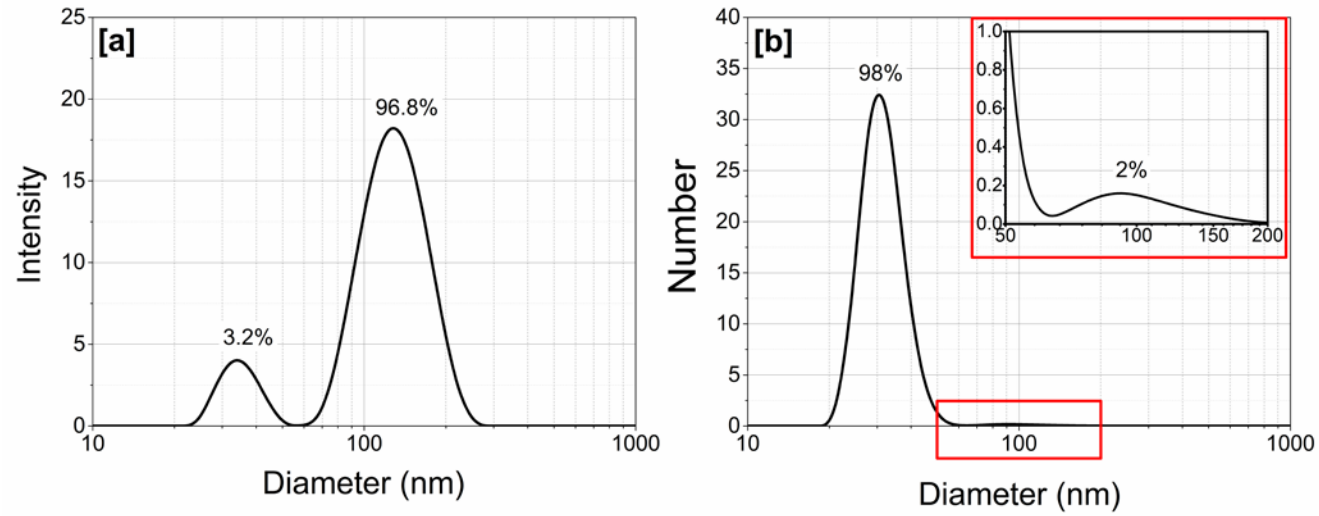

Figure 1) nZVSI DLS size distribution in intensity (a) and number (b), relative abundance was obtained with peak integration

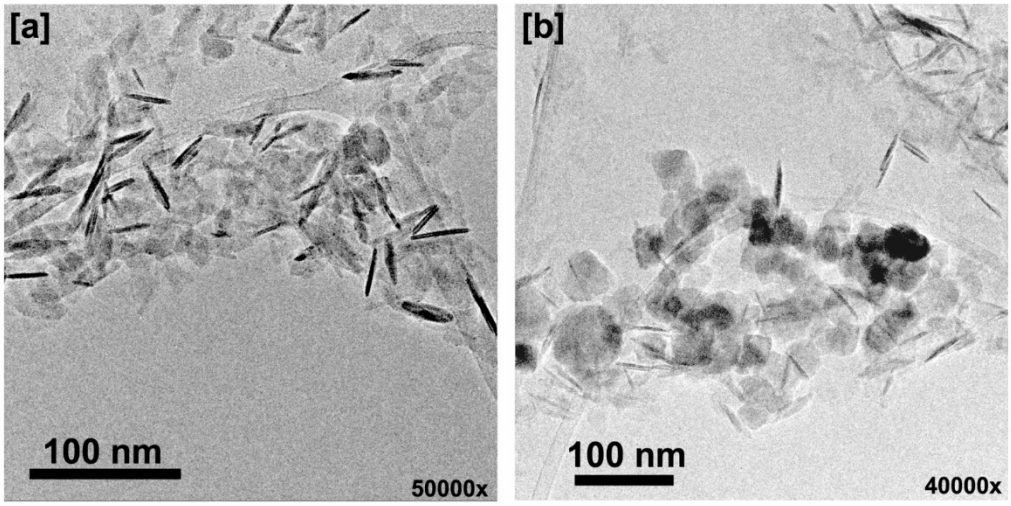

Figure 2) TEM images of washed nZVSI at 50000x (a) and 40000x (b) magnification, sample dried in air on copper mesh grid

From the TEM images collected at magnification 50000x (Figure 2a) and 40000x (Figure 2b) processed using ImageJ (Schneider et al., 2012), two main morphologies can be observed: *i*) pseudo-spherical (≈62% in number): average diameter 38±2 nm, *ii*) acicular (≈38% in number): average length 32±1.4 nm, average width 4±0.2 nm. From these observations, the main geometry appears to be platelet-like, as the acicular particles length was similar to the diameter of the pseudo-spherical particles, and their colour darker. It is worth noticing that both DLS and TEM analyses support the nanometric size of the materials, which is an important requirement for fast degradation activities during site remediation, as the reaction rate is higher at larger values of the specific surface area. The agglomerate size (122 nm) was also very close to the nanometric range. The platelets morphology is generally attributed to iron oxides formed after nZVI aging (Torrey et al., 2015), but it must be pointed out that the samples were sonicated and dried in air prior to TEM analyses. This protocol may contribute to the partial oxidation of the material, hence to a change in structure.

The other two monometallic materials were also analysed in terms of size, although with a reduced level of detail. nZVI (see Data in Brief, Figure 1) showed a slightly larger hydrodynamic size compared to the bimetallic product, with a bimodal distribution at 44±2nm (93.3%) and 136±6 nm (6.7%). The TEM analysis showed again a platelet-like structure, but with a side thinner than that observed for nZVSI. Also, an amorphous phase was identified, which covered the particles and sometimes incorporated agglomerates, also preventing the use of TEM imaging for proper dimensional analysis. On ZVS (see Data in Brief, Figure 2), DLS analysis was performed on a sample heavily sonicated to promote the deagglomeration of the particles. Although a primary particle diameter of abt. 43 nm was identified, a significant agglomerate fraction was present (19.3%) with an average size of 230 nm. Due to fast aggregation, the measurement was only

partially reliable. Therefore, the ZVS particles were also analysed using TEM, obtaining an average diameter for primary particles of 48±2 nm. Aggregates were analysed on an air-dried sample using optical microscopy (Optika S-102L, magnification 10x) (see Data in Brief, Figure 3) and had diameters in the range 250-500 μm.

3.3. Chemical properties

As the material was subject to fast oxidation in air (the particles turned from black to brown-red in few minutes of air exposure), an accurate chemical characterization was needed on samples prepared with minimal handling. However, a preliminary discussion is presented based on the EDX spectra retrieved during the TEM analysis, where the element ratio is derived from the peak ratio for the same energy line (K or L). Figure 3 displays the EDX spectra obtained as survey on the whole area of Figure 2b (for more details, please see Data in Brief, Figure 5).

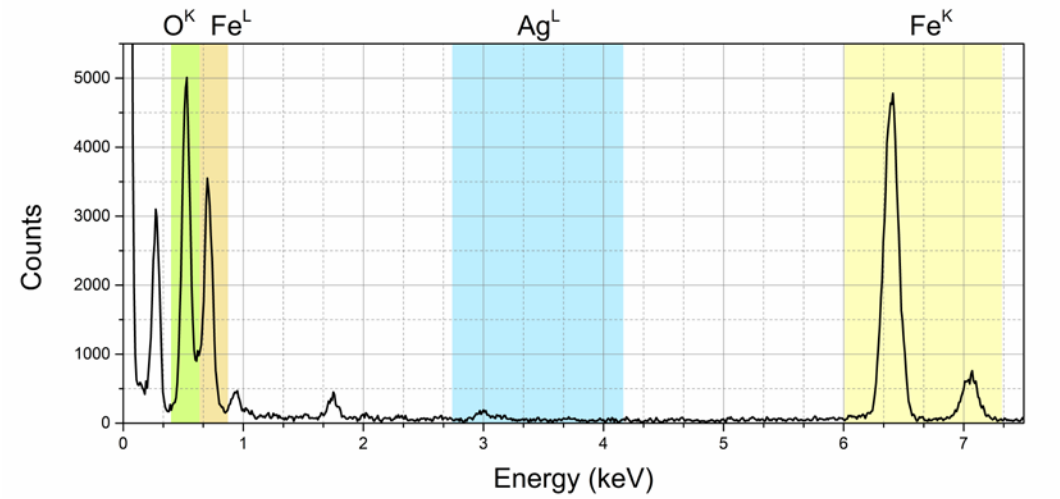

Figure 3) EDX spectra obtained during the TEM analysis, the signal is obtained from the whole area framed in Figure 2b. The peaks without labels are, left to right, carbon, copper and silica.

As no L-lines for oxygen and no K-lines for Ag are available, only Ag:Fe (using L-lines) and Fe:O (using K-lines) ratios can be derived. The non-labelled peaks are generated from the mesh grid (carbon and copper) and the detector (silica). The ratio Ag^L:Fe^L=1:5 is in good accordance with the reactant ratio used during the synthesis (1:5.5). This result also suggests that silver was homogeneously distributed in the material and did not form a significant amount of clusters isolated from the iron phase. In the analysis of two different samples with TEM, only two clusters were found, consisting of less than five silver nanoparticles (see Data in Brief, Figure 6). The ratio Fe^K:O^K=1:0.46 can be compared with the different iron oxides stoichiometries. The lowest iron:oxygen stoichiometric ratio for oxides is 1:1 (related to FeO), while all other iron oxides

present a higher oxygen content. Hence, the oxygen defect registered by the EDX peak ratio supports our claim of having indeed obtained zero-valent iron.

The XPS analysis allowed the obtainment of a more detailed chemical characterization of the product, also including the speciation for both Fe and Ag. Four different samples (1a, 1b, 2a, 2b) were analysed, where the sample number refers to the production batch and the letter to the sample loading procedure (please see Data in Brief, Table 1 for details). For all the samples, the signals from Fe(2p) and Ag(3d) were retrieved; Figure 4 reports the data from sample '2a' (please, see Data in Brief, Figure 7 for O(1s) and S(2p) orbitals and S.I. Table 1 for detailed data on all samples). The sample as received presented a signal for Fe(2p) typical of a mix Fe(II)/Fe(0) with a majority of iron oxide. After the Ar^+ sputtering and the removal of the outer shell, the signal for zero-valent iron (706 eV, green arrow in Figure 4) increased.

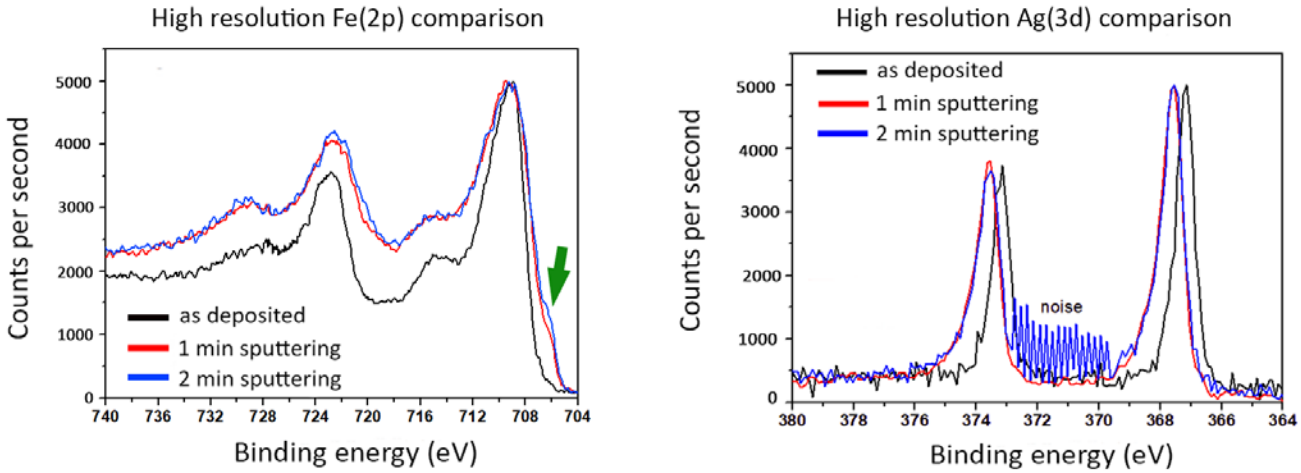

Figure 4) XPS analysis of sample 2a for orbitals Fe(2p) and Ag(3d) of the sample as received (black), after 1 minute (red) and 2 minutes (blue) of Ar^+ sputtering. For Fe(2p) main peaks are $p_{3/2}$ 709.3 eV and $p_{1/2}$ 722.4 eV while satellites peaks are $p_{3/2}$sat 715.1 eV and $p_{1/2}$sat 728.4 eV. For Ag(3d) peaks are $d_{5/2}$ 367.3 eV and $d_{3/2}$ 373.5 eV. Blue shift in Ag(3d) after sputtering leads to $d_{5/2}$ 368.1 eV and $d_{3/2}$ 374.2 eV

The relative abundance of ZVI was 1-5% in the different samples. Using the model proposed by Martin et al. (2008) the thickness of the corresponding oxide layer can be computed. The average thickness on the four samples was 3.52±0.34 nm. Such value is in good agreement with the thickness usually observed upon natural oxidation (3.4±0.7 nm) (Mathieu et al., 1985). The Ag(3d) orbital suggested that the outer shell was composed by a mix of Ag_2O and metallic silver, while after sputtering only Ag(0) was observed, resulting in a blue-shift of the peaks. As no variation in the intensity of the peaks was observed, it can be concluded that Ag was uniformly distributed in the material, a result that corroborates the EDX analyses discussed above and that represents an advantage in terms of silver availability during material deployment, compared to the presence of clusters.

3.4. Reactivity of the bimetallic nZVSI material

Bromophenol blue (BPB) degradation was tested using all the synthesized particles to assess whether the new synthesis protocol grants better performances to the final material. The control sample (BPB with addition of 0.5 mL surnatant) did not show any non-negligible decrease in absorbance over four hours, hence no hydrosulfite residue was present or active. Therefore, the observed degradations can be attributed solely to the reactive material. The degradation kinetics of nZVSI presented in Figure 5a suggest that *i)* nZVSI can completely decolorize BPB and *ii)* decolorization efficiency depended on the mass of added nanoparticles in the BPB solution. From the data in Figure 5b, two ranges can be identified: below 0.8 g/L, nZVSI was not able to completely remove BPB, while above this threshold of mass value the removal was nearly complete.

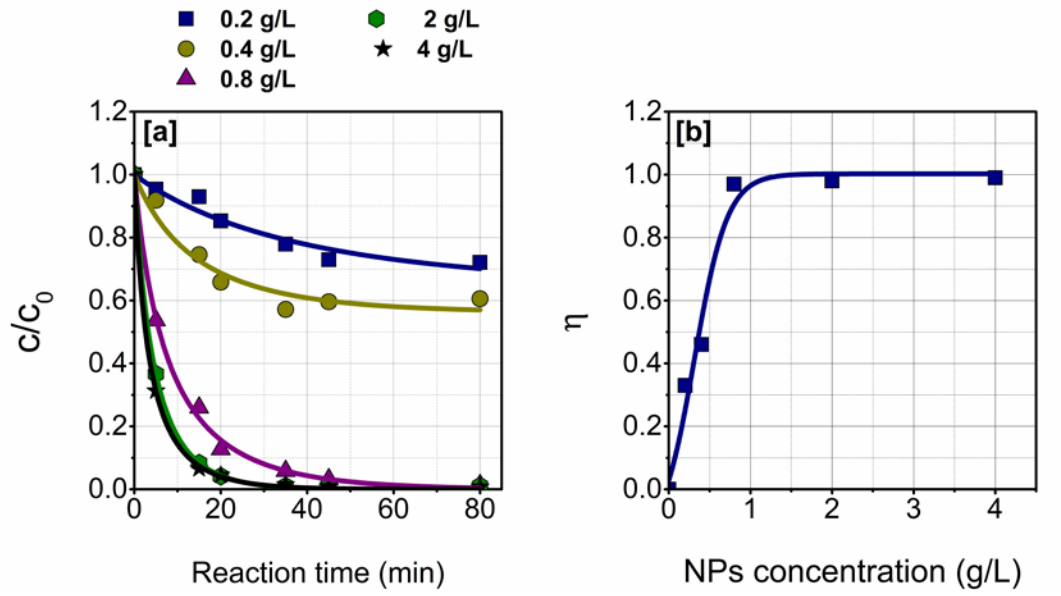

Figure 5) Degradation kinetics of Bromophenol Blue with different mass of nZVSI fitted with the devised model (a); efficiency η fitted by a dose-response model dependency on nanoparticle initial concentration (b)

Using the second-order kinetics equations for both the consumptions of dye and nanoparticles, all possible cases are taken into account, namely stoichiometric ratio of reagents, excess of dye and excess of NPs. Instead of using the second order integrated law, a system with the following two equations was defined:

$$\begin{cases} \frac{dc(t)}{dt} = -k \cdot s \cdot c \\ \frac{ds(t)}{dt} = -h \cdot c \cdot s \end{cases}$$

where “c” is the dye concentration (mol/L), “k” the observed kinetics constant for the dye (L/mol s), “s” the nanoparticle concentration (g/L) and “h” the observed kinetics constant for the reactive material (L/g s). The solution to such system was obtained using Mathematica (Wolfram, 2017).

$$c = c_0 \frac{(ks_0 - hc_0)}{ks_0 e^{(ks_0 - hc_0)t} - hc_0} \;\; ; \;\; s = s_0 \frac{(ks_0 - hc_0) e^{(ks_0 - hc_0)t}}{ks_0 e^{(ks_0 - hc_0)t} - hc_0}$$

To present the data for an immediate understanding, the two equations were then normalized by the initial concentration of dye (c_0) and nanoparticles (s_0), respectively. The same model was also deployed to perform a comparison between the performance of bimetallic nZVSI and the other reactive materials (i.e., nZVI, ZVS).

The model accurately described the data displayed in Figure 5a, setting “c_0” equal to 0.037 mM for all tests (within experimental error) and “s_0” according to the initial concentration of nanoparticles. From the fitting of the model, the value “$k \cdot s_0$” (1/s) was obtained, which represents the kinetics constant at the initial time of the reaction. From the experimental value of the residual concentration at steady state (c_{fin}), the decolorization efficiency η (as $1-c_{fin}/c_0$) and the removal capacity $\varphi^{MAX}=(c_0-c_{fin})/s_0$, i.e., the amount of BPB degraded by a unit mass of reactive nanoparticle were determined. All these data are reported in Table 1 and were used to quantify the performance of nZVSI, and to compare it to that of of ZVS and nZVI.

Table 1) Values for global kinetic constant “k·s0”, decolorization efficiency (η%) and removal capacity at steady state (φMAX) for the different masses for nZVS tested

nZVSI (g/L)	**$k \cdot s_0$ (1/s)**	**η% [a]**	**φ^{MAX} [b] (mg_{DYE}/g_{NP})**
0.2	0.01	30%	32.1
0.4	0.034	43%	29.8
0.8	0.145	>99%	>31.8
2	0.250	>99%	(12.7) [c]
4	0.336	>99%	(6.4) [c]

[a] η% obtained as $(1-c_{fin}/c_0)$, where c_{fin} refers to the steady-state and c_0 to the initial concentration of dye; [b] φ^{MAX} obtained as $(c_0-c_{fin})/s_0$, where c_{fin} refers to the steady-state and c_0, s_0 to the initial concentration of dye and nanomaterial respectively; [c] Data in brackets as the excess of reactive material does not allow a correct computation of effective removal capacity

The kinetics constant "$k \cdot s_0$" monotonously increased with the increase in nZVSI concentration. As for the removal capacity at steady state (φ^{MAX}, mg_{DYE}/g_{NPs}), an average value equal to 31.2±0.7 mg_{DYE}/g_{NPs} was obtained for a nanoparticle (nZVSI) concentration up to 0.8 g/L. Above such concentration, the removal capacity decreased reaching a value of 6.4 mg_{DYE}/g_{NPs} at 4 g/L (20% of φ^{MAX}). When efficiency is considered, reaching a value of $\eta \approx 1$ corresponded to a nearly complete decrease in φ^{MAX}. This result is ascribed to a stoichiometric excess of nanoparticles with respect to the dye concentration. Hence, the lower calculated φ does not indicate poorer performance, rather that part of the material was still unreacted and available at the end of the test, thus still capable of decolorizing additional BPB. This claim is supported by the decrease in φ^{MAX} for the last two tests: as the nZVSI concentration doubled, a halving in φ^{MAX} occurred. Therefore, the value of removal capacity would likely approach that observed in the presence of excess dye, i.e., 31.2 mg_{DYE}/g_{NPs}, under such conditions. An additional test aimed at understanding the possible contributions of BPB sorption during the tests. To this purpose, a solvent (50% ethanol/water) extraction was performed under sonication of the reactive material at the end of the degradation test. As no dye was retrieved, it can be safely concluded that the decolorization process consisted of degradation rather than mere sorption.

3.5. Reactivity comparison with monometallic materials

The degradation data relative to monometallic particles are reported in Figure 6 for the tests carried out with a particle concentration of 0.8 g/L. It is evident that nZVSI significantly outperformed the monometallic materials. The performances of nZVI and ZVS were also quantified using the value of the observed kinetics constant "$k \cdot s_0$", the efficiency (η), and the mass of dye removed per mass unit of nanoparticles (removal capacity, φ^{MAX}). Such data are summarized in Table 2.

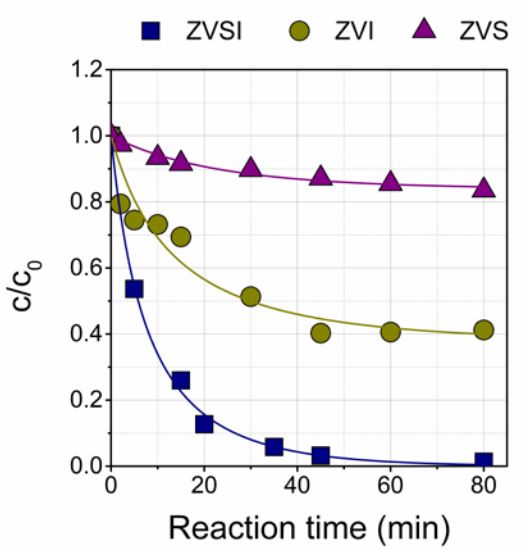

Figure 6) Comparison of degradation BPB decoloured with 0.8 g/L of nZVSI, nZVI and ZVS

Table 2) Values for global kinetic constant "$k \cdot s_0$", decolorization efficiency (η%) and removal capacity at steady state (φ^{MAX}) for the different materials at 0.8 g/L concentration

Material (type)	**$k \cdot s_0$ (1/s)**	**η% [a]**	**φ^{MAX} [b] (mg_{DYE}/g_{NP})**
0.8 g/L nZVSI	0.145	>99%	>31.8
0.8 g/L nZVI	0.065	60%	19.3
0.8 g/L ZVS	0.007	16%	5.1

[a] η% obtained as $(1-c_{fin}/c_0)$, where c_{fin} refers to the steady-state and c_0 to the initial concentration of dye; [b] φ^{MAX} obtained as $(c_0-c_{fin})/s_0$, where c_{fin} refers to the steady-state and c_0, s_0 to the initial concentration of dye and nanomaterial respectively

The results suggest that the efficiency of nZVSI was significantly larger than that of nZVI or ZVS, with a steady state η% value greater than 99% achieved in less than 1 hour, versus 60% and 16%, respectively. The removal capacity, φ^{MAX}, which was 1.7 to 6 times greater for nZVSI compared to the other materials, also highlighted the better performance of the bimetallic nanoparticles. Moreover, as the same amount of metal salts was used in the synthesis of nZVSI and that of the monometallic materials, the fact that the performance for nZVSI was better than the sum of the performance of ZVI and ZVS, suggests that synergistic effects were established between iron and silver. Two main phenomena are proposed that may explain this behaviour *i)* the pre-reduction of silver leading to a lowering of the solution ORP, which thus falls in a pE/pH region where Fe(0) is stable and leads to higher yield in ZVI and lower iron oxide production and *ii)* the doping effect of

silver on iron, with a consequent band-gap shift and possible H_2 production, previously observed also for palladium doping (Yan et al., 2010), with hydrogen acting as a further reductant. This mechanism is interesting and points toward the possibility to further reduce the amount of silver needed in the reactive material, which would translate in an overall cost reduction and less concern for the material toxicity. Therefore, the co-reduction process adopted for the synthesis seems to provide the final product with unique features which are desired for its application in environmental remediation.

4. CONCLUSIONS

The results obtained in our study points toward the possibility to employ hydrosulfite for nZVI production, overcoming the low Fe(0) yield and poor reactivity achieved by other protocols so far. The final material obtained via co-reduction with silver shows nanometric size and suitable reactivity, which was significantly higher than that shown by the monometallic materials on a model pollutant. Although the synthesis proposed here is semi-green, its advantages are evident when we consider that it prevents the production of toxic borates in the final synthesis stage prior to the delivery of nZVI into environment matrices. This achievement significantly reduces the concerns over the product (indirect) toxicity and eliminates the need of cumbersome downstream purification and the disposal of the toxic wastes. Given the fact that a single nanoremediation application requires hundreds of thousands of kilograms of material, this effect is of significant benefit.

Additional benefits are related to the proposed protocol, other than those related to site remediation activities. Since explosive risk is also eliminated during synthesis, the protocol does not require specialized facilities, and the nanoparticles may be injected into a contaminated aquifer following synthesis performed directly on-site. In this implementation, the nanoremediation would take advantage also of the hydrosulfite residues, which would act as reducing agents *i)* directly on the pollutant, thus increasing the removal efficiency and *ii)* on the reactive nanoparticles, slowing down ageing and thus prolonging the lifetime of the reactive particles. Such possibility is particularly interesting, promoting a near zero-waste synthesis, as all the water and the reagents used in the synthesis would be employed in the remediation and not discharged as waste.

A preliminary cost analysis based solely on the cost of reagents for bulk purchases (>10 tons), evidenced how the use of silver should not affect excessively the final price of nZVSI. The average price would be equal to 17 €/kg. When different Ag:Fe ratios are considered, the price of nZVSI would vary from 15 to 25 €/Kg, a range comparable with the cost of commercial zero-valent iron nanoparticles. In the perspective of upscaling this new method, the potential toxic effects of silver

towards aquatic organisms and humans should also be considered. In particular, a comparative study between nZVSI and commercial nanoparticles synthesized using borohydride may provide additional information on the benefits and shortcomings of the proposed method (Corsi et al., 2018). Further studies are also needed to assess whether nZVSI is actually able to remove other and more significant pollutants, and to evaluate the by-product toxicity.

Acknowledgment

The Authors would like to thank Dr. Maria Carmen Valsania from Università degli Studi di Torino for her assistance in the TEM analysis; Dr. Micaela Castellino from CSHR - Center for Space Human Robotics of Istituto Italiano di Tecnologia for assistance in XPS analysis.

Supporting Information. Supporting information on monometallic materials characterization and additional XPS data for nZVSI are available as Data in Brief

REFERENCES

Bates, M.E., Grieger, K.D., Trump, B.D., Keisler, J.M., Plourde, K.J., Linkov, I., 2016. Emerging Technologies for Environmental Remediation: Integrating Data and Judgment. Environmental Science & Technology 50(1), 349-358.

Cary, C.F., Hybinette, S.E., 1947. Thermal reduction of metals. Hybinette and Cary, United States.

Chao, M.S., 1986. The Sulfite/Dithionite Couple: Its Standard Potential and Pourbaix Diagram. Journal of The Electrochemical Society 133(5), 954-955.

Corsi, I., Winther-Nielsen, M., Sethi, R., Punta, C., Della Torre, C., Libralato, G., Lofrano, G., Sabatini, L., Aiello, M., Fiordi, L., Cinuzzi, F., Caneschi, A., Pellegrini, D., Buttino, I., 2018. Ecofriendly nanotechnologies and nanomaterials for environmental applications: Key issue and consensus recommendations for sustainable and ecosafe nanoremediation. Ecotoxicology and Environmental Safety 154, 237-244.

Cox, E., Durant, N., 2005. Nanoscale iron: an emerging technology for in situ treatment of halogenated organics and heavy metals in groundwater. unpublished work.

Crane, R.A., Scott, T.B., 2012. Nanoscale zero-valent iron: Future prospects for an emerging water treatment technology. Journal of Hazardous Materials 211-212(Supplement C), 112-125.

Di Molfetta, A., Sethi, R., 2006. Clamshell excavation of a permeable reactive barrier. Environmental Geology 50(1), 361-369.

Di Vincenzo, M., Barboiu, M., Tiraferri, A., Legrand, Y.M., 2017. Polyol-functionalized thin-film composite membranes with improved transport properties and boron removal in reverse osmosis. Journal of Membrane Science 540, 71-77.

Duydu, Y., Basaran, N., Bolt, H.M., 2016. Reproductive toxicity of boric acid and sodium borates. Toxicology Letters 258(Supplement), S29.

Fazlzadeh, M., Rahmani, K., Zarei, A., Abdoallahzadeh, H., Nasiri, F., Khosravi, R., 2017. A novel green synthesis of zero valent iron nanoparticles (NZVI) using three plant extracts and their efficient application for removal of Cr(VI) from aqueous solutions. Advanced Powder Technology 28(1), 122-130.

Fu, F., Dionysiou, D.D., Liu, H., 2014. The use of zero-valent iron for groundwater remediation and wastewater treatment: A review. Journal of Hazardous Materials 267(Supplement C), 194-205.
Harutyunyan, A., Grigorian, L., Tokune, T., 2005. Method for synthesis of metal nanoparticles. Honda Motor Co., Ltd., United States.
Hashim, M.A., Mukhopadhyay, S., Sahu, J.N., Sengupta, B., 2011. Remediation technologies for heavy metal contaminated groundwater. Journal of Environmental Management 92(10), 2355-2388.
Heindel, J.J., Price, C.J., Schwetz, B.A., 1994. The developmental toxicity of boric acid in mice, rats, and rabbits. Environmental Health Perspectives 102(Suppl 7), 107-112.
Hwang, Y.-H., Kim, D.-G., Shin, H.-S., 2011. Effects of synthesis conditions on the characteristics and reactivity of nano scale zero valent iron. Applied Catalysis B: Environmental 105(1), 144-150.
Kozma, G., Rónavári, A., Kónya, Z., Kukovecz, Á., 2016. Environmentally Benign Synthesis Methods of Zero-Valent Iron Nanoparticles. ACS Sustainable Chemistry & Engineering 4(1), 291-297.
Kumar, R., Singh, N., Pandey, S.N., 2015. Potential of green synthesized zero-valent iron nanoparticles for remediation of lead-contaminated water. International Journal of Environmental Science and Technology 12(12), 3943-3950.
Li, D., Ji, G., Hu, J., Hu, S., Yuan, X., 2018. Remediation strategy and electrochemistry flushing & reduction technology for real Cr(VI)-contaminated soils. Chemical Engineering Journal 334(Supplement C), 1281-1288.
Ma, X., He, D., Jones, A.M., Collins, R.N., Waite, T.D., 2016. Reductive reactivity of borohydride- and dithionite-synthesized iron-based nanoparticles: A comparative study. Journal of Hazardous Materials 303(Supplement C), 101-110.
Maretto, M., Vignola, R., Williams, C.D., Bagatin, R., Latini, A., Petrangeli Papini, M., 2015. Adsorption of hydrocarbons from industrial wastewater onto a silica mesoporous material: Structural and thermal study. Microporous and Mesoporous Materials 203(C), 139-150.
Martin, J.E., Herzing, A.A., Yan, W., Li, X.-q., Koel, B.E., Kiely, C.J., Zhang, W.-x., 2008. Determination of the Oxide Layer Thickness in Core−Shell Zerovalent Iron Nanoparticles. Langmuir 24(8), 4329-4334.
Mathieu, H.J., Datta, M., Landolt, D., 1985. Thickness of natural oxide films determined by AES and XPS with/without sputtering. Journal of Vacuum Science & Technology A: Vacuum, Surfaces, and Films 3(2), 331-335.
Minella, M., Sappa, E., Hanna, K., Barsotti, F., Maurino, V., Minero, C., Vione, D., 2016. Considerable Fenton and photo-Fenton reactivity of passivated zero-valent iron. RSC Advances 6(89), 86752-86761.
Mueller, N.C., Braun, J., Bruns, J., Černík, M., Rissing, P., Rickerby, D., Nowack, B., 2012. Application of nanoscale zero valent iron (NZVI) for groundwater remediation in Europe. Environmental Science and Pollution Research 19(2), 550-558.
Münchow, V., Steudel, R., 1994. The Decomposition of Aqueous Dithionite and its reactions with polythionates SnO2−6 (n = 3–5) studied by ion-pair chromatography. Zeitschrift für anorganische und allgemeine Chemie 620(1), 121-126.
Mystrioti, C., Xanthopoulou, T.D., Tsakiridis, P., Papassiopi, N., Xenidis, A., 2016. Comparative evaluation of five plant extracts and juices for nanoiron synthesis and application for hexavalent chromium reduction. Science of The Total Environment 539(Supplement C), 105-113.
Novak Jovanović, I., Miličević, A., 2017. A model for the estimation of oxidation potentials of polyphenols. Journal of Molecular Liquids 241(Supplement C), 255-259.
Remy, P., Muhr, H., Plasari, E., Ouerdiane, I., 2005. Removal of boron from wastewater by precipitation of a sparingly soluble salt. Environ Prog 24(1), 105-110.
Sadik, O.A., Noah, N.M., Okello, V.A., Sun, Z., 2014. Catalytic Reduction of Hexavalent Chromium Using Palladium Nanoparticles: An Undergraduate Nanotechnology Laboratory. Journal of Chemical Education 91(2), 269-273.
Saleh, N., Sirk, K., Liu, Y., Phenrat, T., Dufour, B., Matyjaszewski, K., Tilton, R.D., Lowry, G.V., 2007. Surface Modifications Enhance Nanoiron Transport and NAPL Targeting in Saturated Porous Media. Environmental Engineering Science 24(1), 45-57.

Schaeffer, G.W., Waller, M.C., Hohnstedt, L.F., 1961. Aqueous Sodium Borohydride Chemistry. Lead, Barium, Mercury, Cadmium, and Zinc. Analytical Chemistry 33(12), 1719-1722.
Schlesinger, H.I., Brown, H.C., Finholt, A.E., Gilbreath, J.R., Hoekstra, H.R., Hyde, E.K., 1953. Sodium Borohydride, Its Hydrolysis and its Use as a Reducing Agent and in the Generation of Hydrogen1. Journal of the American Chemical Society 75(1), 215-219.
Schneider, C.A., Rasband, W.S., Eliceiri, K.W., 2012. NIH Image to ImageJ: 25 years of image analysis. Nat Meth 9(7), 671-675.
Stefaniuk, M., Oleszczuk, P., Ok, Y.S., 2016. Review on nano zerovalent iron (nZVI): From synthesis to environmental applications. Chemical Engineering Journal 287(Supplement C), 618-632.
Sunardi, Ashadi, Sentot Budi, R., Inayati, 2017. Ecofriendly Synthesis of nano Zero Valent Iron from Banana Peel Extract. Journal of Physics: Conference Series 795(1), 012063.
Torrey, J.D., Killgore, J.P., Bedford, N.M., Greenlee, L.F., 2015. Oxidation behavior of zero-valent iron nanoparticles in mixed matrix water purification membranes. Environmental Science: Water Research & Technology 1(2), 146-152.
Tosco, T., Petrangeli Papini, M., Cruz Viggi, C., Sethi, R., 2014. Nanoscale zerovalent iron particles for groundwater remediation: a review. Journal of Cleaner Production 77, 10-21.
Wolfram, 2017. Wolfram Research, Inc., Mathematica, Version 11.2, Champaign, IL (2017).
Xu, Y., Jiang, J.-Q., 2008. Technologies for Boron Removal. Industrial & Engineering Chemistry Research 47(1), 16-24.
Yan, W., Herzing, A.A., Li, X.-q., Kiely, C.J., Zhang, W.-x., 2010. Structural Evolution of Pd-Doped Nanoscale Zero-Valent Iron (nZVI) in Aqueous Media and Implications for Particle Aging and Reactivity. Environmental Science & Technology 44(11), 4288-4294.
Yin, W., Ai, J., Huang, L.-Z., Tobler, D.J., B. Hansen, H.C., 2018. A Silicate/Glycine Switch To Control the Reactivity of Layered Iron(II)–Iron(III) Hydroxides for Dechlorination of Carbon Tetrachloride. Environmental Science & Technology 52(14), 7876-7883.
Zhang, W.X., 2003. Nanoscale iron particles for environmental remediation: An overview. Journal of Nanoparticle Research 5(3-4), 323-332.
Zhao, X., Liu, W., Cai, Z., Han, B., Qian, T., Zhao, D., 2016. An overview of preparation and applications of stabilized zero-valent iron nanoparticles for soil and groundwater remediation. Water Research 100(Supplement C), 245-266.